Studies of Liquid−Vapor Equilibria, Criticality, and Spinodal Transitions in Nanopores by the Gauge Cell Monte Carlo Simulation Method

Aleksey Vishnyakov and Alexander V. Neimark*

TRI/Princeton, 601 Prospect Avenue, Princeton, New Jersey 08542

Received: October 27, 2000; In Final Form: April 9, 2001

Liquid−vapor equilibrium, criticality, and spinodal transitions in nanopores are studied by the gauge cell Monte Carlo simulation method proposed recently (Neimark, A. V.; Vishnyakov, A. *Phys. Rev. E* **2000**, *62*, 4611). As an instructive example, we consider the capillary condensation of argon in cylindrical pores of different diameters (1.5−5.5 nm) representing typical pore channels in mesoporous molecular sieves. At the subcritical conditions, the gauge cell method allows one to construct continuous phase diagrams in the form of a van der Waals-type sigmoid isotherm. The sigmoid isotherm contains stable and metastable states on the adsorption and desorption branches connected by a backward trajectory of thermodynamically unstable states which cannot be observed experimentally yet can be stabilized in simulations. The phase equilibrium is determined by thermodynamic integration along the sigmoid trajectory using the Maxwell rule. The spinodals give the true limits of stability of vaporlike and liquidlike states. A notable difference was found between the spinodals and the limits of stability of the vaporlike and liquidlike states achieved in grand canonical Monte Carlo simulations. The critical conditions of the first-order vapor−liquid transition in pores were determined. Good agreement with experimental data on argon adsorption at 87 K on mesoporous molecular sieves was found for equilibrium transitions in pores wider than 2.2 nm and for hysteretic adsorption−desorption isotherms in pores wider than 5 nm.

1. Introduction

The molecular modeling of phase transitions and criticality in nanometer-scale pores has received a great deal of attention in view of recent remarkable progress in synthesis and practical utilization of nanomaterials such as mesoporous molecular sieves, carbon nanotubes, and polymer nanofibers. Monte Carlo simulations, primarily the grand canonical (GCMC) and Gibbs ensemble (GEMC) methods, were successfully employed to explain the specifics of liquid−vapor transitions,[2−9] liquid−liquid equilibrium,[10,11] and freezing[2,12,13] in pores of a few molecular diameters in width; for the most recent review see ref 14. Confined systems are characterized by multiple metastable states and associated hysteresis phenomena.[14,15] To study a system with multiple stable and metastable states, one has to impose certain constraints to scan a limited area of the system configuration space.[16,17] To investigate metastability in bulk systems, different versions of the restricted ensemble have been introduced.[18,19] As related to the confined systems, the statistical mechanical analysis is hindered[20] and no rigorous simulation procedures were considered. In our previous communication,[1] we have introduced a new method, named the gauge cell method, which extends capabilities of traditional simulation techniques such as GCMC and GEMC. The gauge cell method allows one to determine the equilibrium transition and also the true limits of stability (spinodals) of metastable phases. The method is based on the construction of a continuous isothermal trajectory of equilibrium states in the form of a van der Waals loop, which includes thermodynamically stable, metastable, and unstable states. The thermodynamically unstable states, which cannot be obtained in experiments, are stabilized in simulations by suppressing the density fluctuations in the system. It is worth noting that while the feasibility of unstable states generation in the MD and MC simulations was shown previously,[21,22] no attempt has been made to use the trajectory of unstable states to calculate the thermodynamic functions in metastable and stable states. In the proposed method,[1] the thermodynamic functions of equilibrium states are determined by thermodynamic integration along the metastable and unstable regions of the isotherm. Then, the conditions of phase coexistence are calculated employing the Maxwell rule of equal areas. In doing so, the energy barrier separating the metastable and stable states and, correspondingly, the probability of spontaneous phase transitions can also be estimated. Although a strict statistical mechanical analysis of the gauge cell method and its limitations is still in the works, the agreement with the proven techniques of GCMC and GEMC simulations and also with some reference experiments[1] is quite convincing.

In this paper, we apply the gauge cell MC method to study liquid−vapor equilibrium, criticality, and spinodal transitions in nanopores. As an instructive example, we consider the capillary condensation of argon at its boiling temperature 87 K in cylindrical nanopores representing pore channels in siliceous mesoporous molecular sieves. This choice was motivated by the availability of reliable experimental data, which provides an opportunity to validate the simulation results. The paper is structured as follows. In section 2, we describe the gauge cell method and simulation details. In section 3, we present two series of simulations of equilibrium sorption of the Lennard-Jones fluid with parameters of argon in cylindrical pores representing the channels of MCM-41 materials and determine the critical conditions, equilibrium, and spinodal transitions. The temperature dependence of capillary condensation was studied for argon sorption in a pore of 2.2 nm diameter, at temperatures from 57 to 105 K. The pore size dependence was studied at argon boiling temperature 87 K in a series of pore channels ranging from 2.2 to 5.5 nm. We compare the results of the gauge

* Author for correspondence. E-mail: aneimark@triprinceton.org.

10.1021/jp003994o CCC: $20.00
Published on Web 06/20/2001

cell method with the sorption isotherms obtained by the GCMC simulation. In section 4, we compare the simulated isotherms with experimental data collected on well-characterized samples of MCM-41 type materials. In section 5 we calculate the energy barriers separating the metastable and stable states and, correspondingly, the probability of spontaneous phase transitions. In section 6, we summarize the results and conclude that the gauge cell method is efficient for studies of phase transitions and criticality in confined systems.

2. The Gauge Cell Method and Simulation Details

2.1. Construction of the Continuous Adsorption Isotherm. The gauge cell method[1] as related to the liquid−vapor equilibrium in pores involves construction of a continuous adsorption isotherm, which includes not only stable and metastable equilibrium states but also a sequence of thermodynamically unstable states. The unstable equilibrium states, which cannot be observed experimentally, are stabilized in simulations by suppressing the range of admissible density fluctuations. This is the key point of the gauge cell method. Simulation is performed simultaneously in two cells, which are in thermal equilibrium with an infinite heat bath, Figure 1a. One of the cells represents a pore, and the other is a gauge cell of a limited capacity. It is assumed that the equation of state of the fluid in the gauge cell is known or can be obtained independently. Thus, the gauge cell fluid serves a reference. We allow mass exchange between the cells; however, the cell volumes are kept unchanged. That is, we do not require mechanical equilibrium between the cells, similar to the pore-fluid GEMC method.[6] Due to this analogy, the proposed method can be referred to as the pore-gauge GEMC method.[1] Note that the statistical ensemble under consideration is the canonical ensemble for the total system of two simulation cells. The conditions of isothermal equilibrium imply the equality of chemical potentials in the pore fluid and in the reference fluid. In the subsequent discussion we will refer to the proposed method as the gauge cell method.

The limited capacity of the gauge cell constrains the density fluctuations in the pore and allows one to keep the fluid in the pore in a state that would be unstable in contact with the bulk. Indeed, the determination of the equilibrium distribution of a given number, N_Σ, of molecules between two cells is determined by minimization of the total Helmholtz free energy F_Σ in the canonical ensemble:

$$F_\Sigma = F(N,V,T) + F_g(N_g,V_g,T) \Rightarrow \min \tag{1}$$

at the conditions

$$N_\Sigma = N + N_g = \text{const};\ V,\ V_g,\ T = \text{const} \tag{2}$$

Here and below, the quantities without a subscript are referred to the pore cell, while quantities with the subscript "g" are referred to the gauge cell; F is the Helmholtz free energy, N is the number of molecules, V is the cell volume, and T is the temperature. The condition (1) of the total Helmholtz free energy minimum leads to the equilibrium condition, given by the equality of the chemical potential, μ, of the pore fluid and that of the gauge fluid

$$\mu = (\partial F/\partial N)|_{V,T} = (\partial F_g/\partial N_g)|_{V_g,T} \tag{3}$$

and the stability condition for the total system, given by

$$(\partial^2 F/\partial N^2)|_{V,T} + (\partial F_g/\partial N_g{}^2)|_{V_g,T} > 0 \tag{4}$$

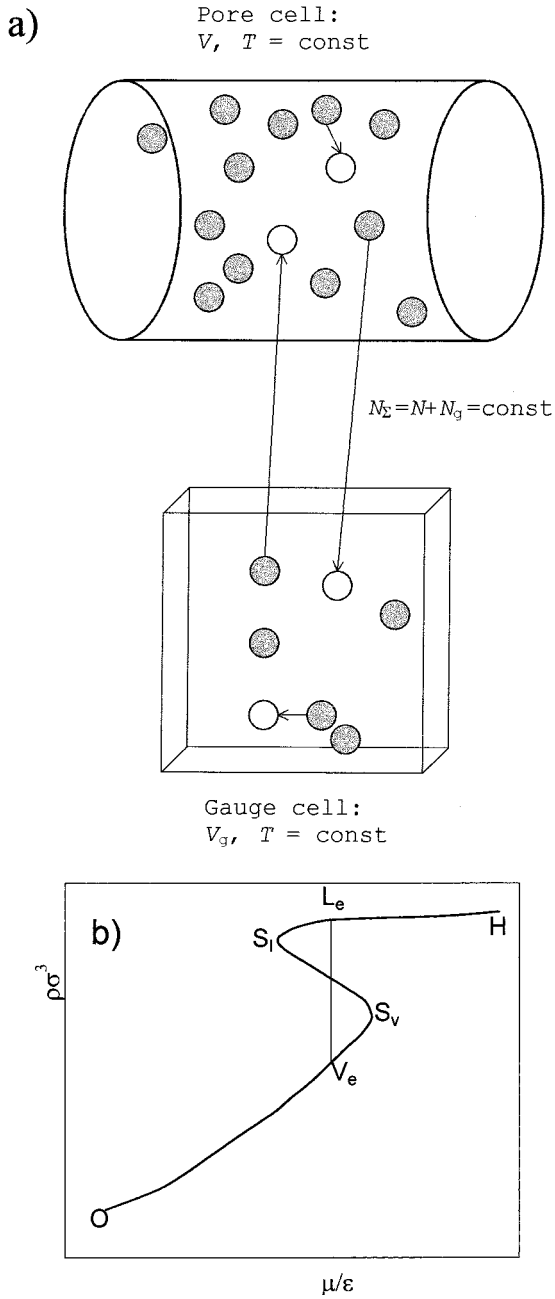

Figure 1. (a) MC simulations in the gauge cell method. The pore cell and the gauge cell of a constant volume are kept in thermal and chemical equilibrium. The allowed types of Monte Carlo steps are (1) displacement of a molecule within the same cell and (2) transfer of a molecule between the cells. (b) Sketch of a full sigmoid adsorption isotherm. O, a low-density vaporlike state where the fluid−fluid interactions are negligible; V_e and L_e, liquidlike and vaporlike states corresponding to the vapor−liquid equilibrium in the pore; S_v and S_l, vaporlike and liquidlike spinodals; H, a stable liquidlike state. The vapor−liquid equilibrium is determined by the Maxwell rule: the shaded areas are equal.

Inequality 4 does not require the fulfillment of the conditions of thermodynamic stability in each of the cells separately. It is assumed that, at the conditions of the simulations, the reference fluid in the gauge cell is stable; i.e., its isothermal compressibility is positive and

$$(\partial^2 F_g/\partial N_g{}^2)|_{V_g,T} = \frac{1}{V_g}\left(\frac{\partial \rho_g}{\partial \mu}\bigg|_T\right)^{-1} > 0 \tag{5}$$

Here ρ_g is the reference fluid density. However, the pore fluid

does not need to be stable. To stabilize an unstable state with a negative compressibility, $(\partial^2 F/\partial N^2)|_{V,T} = (1/V)[(\partial\rho/\partial\mu)|_T]^{-1} < 0$ (ρ is the pore fluid density), one has to choose the gauge cell of a sufficiently small volume. If the reference fluid can be regarded as an ideal gas, as in our simulation of argon equilibrium at 87 K (see details below), the system of the two cells is stable when the ratio of the pore and gauge volumes, V_g/V, complies with the inequality[15]

$$\frac{V_g}{V} < |\frac{\partial\rho}{\partial\mu}|/\frac{\rho_g}{kT} \tag{6}$$

The use of the gauge cell has two functions: *to measure the chemical potential in the equilibrium pore fluid* and *to stabilize the states of negative compressibility*.

Provided inequality 6 is fulfilled, one can construct the continuous sigmoid trajectory of the equilibrium states similar to the van der Waals loop. A scheme of the full adsorption isotherm at subcritical conditions is presented in Figure 1b. The ascending, adsorption branch OS_v describes the formation of the adsorbed film on the pore walls as the vapor pressure in the bulk increases. Since the fluid in the pore center has a density close to that of vapor, these states are referred to as *vaporlike* states. The adsorption branch terminates at the *vaporlike spinodal* S_v, where the isothermal compressibility diverges. The vaporlike spinodal corresponds to the true limit of stability of the adsorbed film. The descending, desorption branch HS_l describes the decrease of the condensed fluid density as the vapor pressure in the bulk decreases. These states are referred to as *liquidlike* states. The desorption branch terminates at the *liquidlike spinodal* S_l, where the isothermal compressibility diverges. The liquidlike spinodal corresponds to the true limit of stability of the liquidlike states. The spinodals are connected by the trajectory of physically unstable states, which are stabilized in the simulation by the presence of the gauge cell. An opportunity to achieve the true limits of stability of the simulated phases and to determine contiguously the chemical potential distinguishes the gauge cell method as a unique tool to study metastable states and spinodal transitions.

It should be noted that all the states constituting the sigmoid isotherm in Figure 1b comply with the confinement symmetry. That is, in the case of cylindrical pores, the local fluid density is translation invariant and does not vary along the pore axis. In confined systems symmetry invariance plays a role similar to that of uniformity in bulk systems: phase separation implies symmetry breaking. In analogy with bulk systems, one may expect that the symmetry-invariant states in the range of densities between the spinodal points are mechanically unstable and, therefore, do not exist. However, the gauge cell method imposes so severe constraints of density fluctuations that we have succeeded in stabilizing the translation-invariant states on the backward trajectory of the isotherm. These states are unstable unless the density fluctuations are sufficiently suppressed. To be precise, the gauge cell method as applied to cylindrical confinements imposes two types of constraints: (1) the density variations are limited due to a small volume of the gauge cell, and (2) the periodic boundary conditions do not allow for a symmetry breaking that is a prerequisite of phase separation. The length of the pore cell is an important factor. Since our goal was to generate a continuous sequence of symmetry-invariant states to close the hysteresis loop between the spinodals, all simulations were performed in the relatively short periodic cell of 10 molecular diameters in length. In so doing, the cell length is smaller than the minimum wavelength of developing density fluctuations.[23] For sufficiently long periodic cells, we expect to get density patterns with phase separation. An analysis of the influence of periodic boundary conditions on density patterns is beyond this work. We also do not attempt to discuss the statistical mechanical foundations of the gauge cell method, which is a symbiosis of the Gibbs ensemble[6] and the restricted ensemble.[16,18,19]

Our further discussion of the capillary condensation in a cylindrical capillary as a first-order phase transition seems to be in an apparent contradiction with the rigorous statistical mechanical conclusion that no phase transition may occur in a one-dimensional system.[24−26] To avoid possible confusions and misinterpretations, note that the Landau theorem[24] forbids thermodynamic equilibrium between two uniform semi-infinite phases, which are situated on a line and have a point contact. We do not consider an infinite system; rather we consider a finite cell with periodic boundary conditions. We also do not consider a real coexistence between two phases separated by an interface. Capillary condensation in a sufficiently long capillary is inevitably associated with formation of a set of liquid droplets bridging the pore cross section and bubbles. According to the classical theory,[24,27] the characteristic distance between phase inclusions is proportional to $\exp(2\pi R^2\gamma/kT)$, where γ is the interfacial tension. This distance far exceeds the length of the simulation cell, and therefore, the generated equilibrium liquidlike and vaporlike states correspond to the central parts of the long phase inclusions, which would be observed in an "infinite" system. In the following discussion, by the phase coexistence in a confined system we mean the conditions at which there exist two equilibrium states of different densities and equal grand thermodynamic potentials. Consequently, by criticality we mean the conditions at which these two states merge and above which (or below, depending on what parameter is varied) there exists only one "supercritical" equilibrium state.

2.2. Determination of the Phase Coexistence Conditions. The true phase equilibrium is achieved somewhere between the spinodals, Figure 1b. Its position is determined from the equality of the grand thermodynamic potentials, $\Omega = F - \mu N$, in the coexisting vaporlike and liquidlike states on the adsorption and desorption branches, respectively:

$$\Omega_a(\mu_e) = \Omega_d(\mu_e) \tag{7}$$

The bulk pressure corresponding to the equilibrium in the pore is obtained from the bulk equation of state, such as the equation of Johnson et al.[28] in the case of a Lennard-Jones (LJ) fluid.

The continuity of the isotherm produced by the gauge cell method allows us to calculate the grand thermodynamic potential $\Omega(\mu)$ in all states along the isotherm. Indeed, integration of the Gibbs equation, $d\Omega = -N\,d\mu$, along the adsorption branch can be extended to the backward trajectory of the constructed S-shaped adsorption isotherm to the desorption branch. Choosing the reference state at a sufficiently small chemical potential μ_r to provide fluid ideality (point O in Figure 1b), one obtains

$$\Omega(\mu,T) = \Omega(\mu_r,T) - \int_{\mu_r}^{\mu} N(\mu,T)\,d\mu = -kTN(\mu_r,T) - \int_{\mu_r}^{\mu} N(\mu,T)\,d\mu \tag{8}$$

In so doing, condition 7 of phase coexistence comes to the Maxwell rule of equal areas:

$$\int_{\mu_e}^{\mu_{sv}} N_a(\mu,T)\,d\mu - \int_{\mu_{sl}}^{\mu_{sv}} N_n(\mu,T)\,d\mu + \int_{\mu_{sl}}^{\mu_e} N_d(\mu,T)\,d\mu = 0 \tag{9}$$

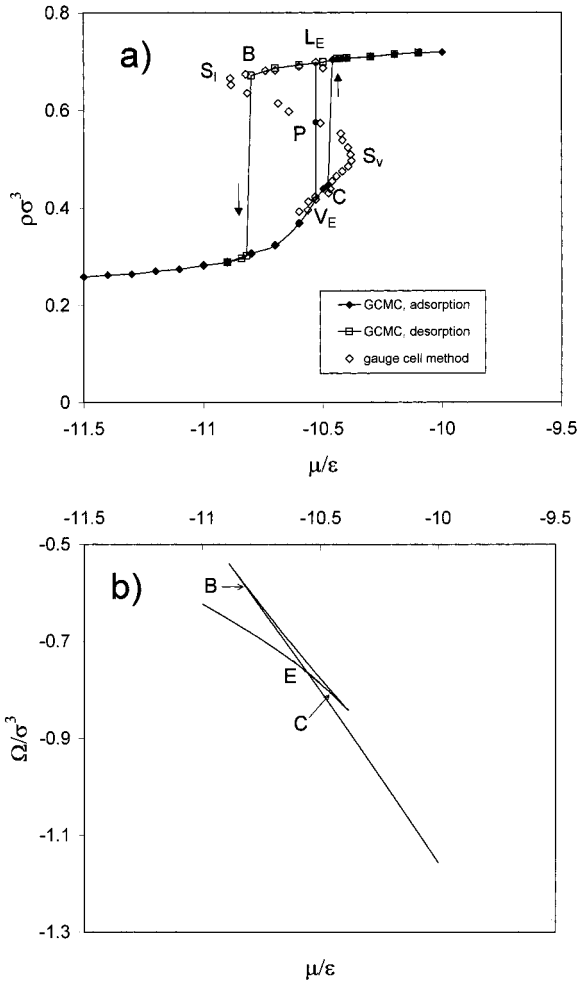

Figure 2. (a) GCMC and gauge cell adsorption isotherms of argon, $kT/\epsilon = 0.73$ (87.3 K), in a 3.60 nm cylindrical pore. Dashed vertical lines show the location of vapor−liquid coexistence in the pore determined by the Maxwell rule: the areas V_ES_vP and PS_lL_E are equal. (b) Isotherm for the grand potential Ω for the same system. Vapor−liquid equilibrium corresponds to the intersection of the vapor and branches (point E). Arrows show the locations of spontaneous liquid−vapor and vapor−liquid transitions in GCMC simulations.

Determination of the conditions of the phase coexistence by thermodynamic integration from eq 9 is a straightforward and precise procedure.

2.3. Comparison of the Gauge Cell and GCMC Simulation Methods. Figure 2 gives an example of the gauge cell and GCMC simulations. We considered adsorption of a LJ fluid in a cylindrical pore of 10 molecular diameters in width. The fluid−fluid and solid−fluid LJ parameters were chosen to model argon in a siliceous cylindrical pore.

The GCGEMC simulation produces a continuous S-shaped trajectory of equilibrium states with the clearly identified vaporlike S_v and liquidlike S_l spinodals. The equilibrium states generated by GCMC coincide with those generated by gauge cell method within a statistical error inherent to MC simulations. However, the GCMC adsorption branch terminated at point C, where the fluid underwent spontaneous capillary condensation. The point of spontaneous condensation differs appreciably from the true stability limit, or the vaporlike spinodal S_v, which is achieved in the gauge cell method. Similarly, the GCMC desorption branch terminated at point B, where the fluid underwent spontaneous evaporation prior to the liquidlike spinodal point S_l achieved by the gauge cell method. To save computation time, it is advantageous, first, to generate stable and metastable states by the less computationally intense GCMC method and then, with some overlap, to extend the metastable state trajectories up to the spinodals and to construct the backward trajectory of unstable states by means of the gauge cell method. Since the states generated by the GCMC simulation and the gauge cell simulation are indistinguishable within inherent errors of both methods, we use all the generated points for the thermodynamic integration.

Integration along the continuous adsorption isotherm in accord with eq 8 gives the isotherm of the grand thermodynamic potential, $\Omega(\mu)$, presented in Figure 2b. The intersection of the adsorption and desorption branches of the grand thermodynamic potential corresponds to the point of phase coexistence, μ_e, eq 7. At this point the Maxwell rule, eq 9, is fulfilled: The areas V_ES_vP and PS_lL_E are equal (Figure 2a).

Note that in case of a stepwise GCMC isotherm, integration in eq 8 can be done along the reversible part of the adsorption isotherm up to the stability limit, where spontaneous condensation was observed. Therefore, to determine the phase coexistence from the GCMC data, one has to perform additional simulations: either to circumvent the spontaneous transitions by a continuous trajectory of equilibrium states in the supercritical region and perform thermodynamic integration as recommended by Peterson and Gubbins[4] or to apply the pore−pore GEMC simulation proposed by Panagiotopoulos.[6] In our previous communication,[1] we have shown using several examples that the numerical results obtained by the gauge cell method (eq 9) agree well with those obtained by the above-mentioned methods. Moreover, the gauge cell method is proved to be more stable and less sensitive with respect to initial conditions and unavoidable fluctuations of the simulation data.

Thus, there are several advantages to using the gauge cell method: First, it is possible to approach the true limits of stability of metastable vaporlike and liquidlike states and to determine precisely the spinodals. Second, generation of the metastable states in the close vicinity of the spinodal may help explain the evolution of spinodal transitions.[29] Third, the use of the Maxwell rule (eq 9) provides a reliable and simple determination of the phase coexistence conditions. Fourth, thermodynamic integration (eq 8) along the trajectory of unstable states allows one to calculate the energy barriers between metastable and stable equilibrium states that helps in better understanding the hysteresis phenomena observed in capillary condensation experiments (see ref 15 and discussion in section 4). Since in the range of applicability of the GCMC method the stable and metastable states generated by both methods do coincide, the less computationally intense GCMC method can be used as a complement to the gauge cell method. One can combine the points generated by both methods into one isotherm.

2.4. Simulation Details. The simulation procedure in the gauge cell method is equivalent to that of the pore-fluid GEMC method.[6,30] We do not consider here the systems of extreme confinement with a small number of molecules, for which the results of simulation may depend on the ensemble employed.[31−33] Two types of MC moves are performed: molecule displacement within the cells and molecule exchange between the cells. In the *displacement step* the cells are independent and represent two unrelated canonical ensembles. A molecule in the pore cell is chosen at random and given a uniform random displacement to a new trial position in the same cell. The trial move is accepted with a probability equal to $\min\{1,\exp(-\Delta E/kT)\}$, where ΔE is the configuration energy change. The same rule is applied to the gauge cell. The *exchange step* consists of an

attempted molecule creation in one of the cells coupled with an attempted molecule destruction in the other cell. The position for the attempted molecule creation and the molecule for the attempted destruction are chosen at random. A trial transfer from the gauge cell to the pore cell is accepted with a probability equal to $\min\{1,\exp(-[\Delta E + \Delta E_g + kT \ln[V_g(N+1)/VN_g]]/kT)\}$. The same rule (with changed subscripts) is applied to a trial transfer from the pore cell to the gauge cell. For a justification of the above acceptance criteria, see ref 30.

In the present work, we apply the gauge cell and GCMC methods to study capillary condensation and desorption of argon in siliceous cylindrical pores representing cylindrical silica channels of MCM-41 at the argon normal boiling temperature, 87.3 K. The Lennard-Jones (LJ) potential with the LJ parameters $\epsilon/k = 119.6$ K and $\sigma = 0.34$ nm and cutoff radius 5σ was used for fluid−fluid interactions. These parameters were determined from the best fit of Johnson's et al.[28] equation of state for LJ fluid to experimental data on vapor−liquid equilibrium for bulk argon.[34]

Following ref 35, the solid−fluid potential in cylindrical pores was modeled as the LJ interaction of adsorbate molecules with the structureless cylindrical layer of adsorption centers on the pore wall:[36]

$$U_{sf}(r,R) = \pi^2 \rho_s \epsilon_{sf} \sigma_{sf}^2 \left\{ \frac{63}{32}\left[\frac{R-r}{\sigma_{sf}}\left(1+\frac{r}{R}\right)\right]^{-10} F\left[-\frac{9}{2},-\frac{9}{2};1;\left(\frac{r}{R}\right)^2\right] - 3\left[\frac{R-r}{\sigma_{sf}}\left(1+\frac{r}{R}\right)\right]^{-4} F\left[-\frac{3}{2},-\frac{3}{2};1;\left(\frac{r}{R}\right)^2\right]\right\} \quad (10)$$

Here, r is the radial coordinate of the adsorbate molecule reckoned from the pore center, $R = H/2$ is the radial coordinate of the adsorption centers, ρ_s is the surface number density of the adsorption centers, and $F[\alpha,\beta;\gamma;\delta]$ is the hypergeometric series. As the pore width increases, this potential reduces to the 10−4 form of the potential with a plane of LJ centers. The parameters of potential (3) were found in ref 37 from the best fit of the calculated argon adsorption isotherm on the flat surface to the experimental isotherm on nonporous silica. Due to the cylindrical shape of the simulation cell, the periodic boundary conditions were applied in the direction parallel to the pore wall. The length of the basic simulation cell was $10\sigma_{ff}$. As the gauge cell, we employed a cube with triply periodic boundary conditions. The size of the gauge cell varied from $30\sigma_{ff}$ to $100\sigma_{ff}$ and was adjusted so that the sufficient number of fluid molecules (>30) was contained in the gauge cell during the simulation. The number of the molecules in the reference cell varied from 30 to 150. Choosing the gauge cell size, one has to compromise between condition (6) and the necessity of providing reliable accuracy in the chemical potential determination. The gauge cell was calibrated by a series of GCMC simulations of the same length as that of the pore simulations. Even for the smallest gauge cell of $30\sigma_{ff}$ in size, the fluid behaved as an ideal bulk vapor. No notable nonideality of the gauge fluid was observed at $\mu < -9.6\epsilon_{ff}$ and $kT/\epsilon_{ff} = 0.73$, which corresponds to the temperature 87.3 K for the fluid−fluid parameters applied. Note that according to the equation of Johnson et al.,[28] the vapor−liquid equilibrium in the bulk LJ fluid at $kT/\epsilon_{ff} = 0.73$ corresponds to $\mu_0 = -9.54\epsilon_{ff}$.

3. Results and Discussion

We have performed two series of simulations of equilibrium sorption of the LJ fluid with parameters of argon in cylindrical pores representing the channels of MCM-41 materials. The temperature dependence of capillary condensation was studied in the temperature range from 57 to 105 K for argon sorption in the pore of 2.2 nm diameter. The pore size dependence was studied at argon boiling temperature, 87 K, in a series of pore channels ranging from 2.2 to 5.5 nm. The choice of the parameters was motivated by availability of relevant experiments.

3.1. Temperature Dependence of Capillary Condensation. Using the gauge cell method, we explored the temperature dependence of argon sorption in the 2.2 nm wide cylindrical pore. This is a typical pore diameter in the MCM-41 sample experimentally studied by Morishige and Shukimi.[38] These authors measured a set of Ar adsorption isotherms at different temperatures. They determined the temperature range of the adsorption hysteresis and, based on an empirical method, estimated the critical temperature of vapor−liquid coexistence as 98 K.

We calculated a series of Ar adsorption isotherms at temperatures from 57 to 105 K, presented in Figure 3a. The 2.2 nm cylindrical pore is able to accommodate three concentric adsorbed layers of argon. In the condensed state, the three-layer structure was observed at all temperatures studied. As expected, the layered structure was more pronounced at lower temperatures. The generated adsorption isotherms are presented in Figure 3. At the lowest temperature 62 K (Figure 3a), the adsorption and desorption branches were obtained by GCMC method. At this temperature, one adsorbed layer is formed at the pore wall prior to capillary condensation. The adsorbed monolayer is very dense with a density of $0.86\sigma^{-2}$ at $\mu = -10.6\epsilon$. This is typical for a two-dimensional hexatic or crystalline phase. At $\mu = -9.6\epsilon$ the fluid condensed and formed a very dense state ($\rho = 0.87\sigma^{-3}$), which may be typical for a glass or even solid state in the pore. In the present work, we do not analyze whether a glass or crystalline state was obtained in the pore. It is worth noting, however, that very few attempts of the particle insertion and removal were successful (about one successful insertion/removal per 5×10^4 attempts at $\mu = -9.6\epsilon$), which makes it difficult to reach equilibrium. For the same reason, the calculations with the gauge cell at such a low temperature are prone to large uncertainties and did not allow us to obtain reliable estimates of the phase coexistence conditions and the spinodals. These difficulties are common in Gibbs ensemble simulations, which are known to be hindered at very high densities. Several methods to avoid these difficulties were proposed in the literature; the discussion can be found elsewhere (e.g., ref 39).

At higher temperatures, the calculations become more reliable. At 87.3 K (Figure 3b) the GCMC isotherms form a very narrow hysteresis loop. However, the full adsorption isotherm obtained by the gauge cell method clearly indicates first-order condensation. The pressures and densities at the spinodal points can be reliably estimated. As the temperature increases, the critical point of vapor−liquid coexistence in the pore is achieved. For example, at 98 K the GCMC isotherm is monotonic and reversible, while the full isotherm obtained by the gauge cell method still has a sigmoid shape (Figure 3c). Based on the latter isotherm, we conclude that the fluid in this pore is still subcritical at 98 K. However, since the system is very close to the critical point, the free energy barrier between the vaporlike and liquidlike phases is so small that it can be overcome by the fluctuations inherent to the GCMC simulations. This means that the average density obtained in the GCMC simulations results from relatively frequent "jumps" from the liquidlike state to the vaporlike state and back. These transitions between liquidlike and vaporlike states are clearly seen along the simulation

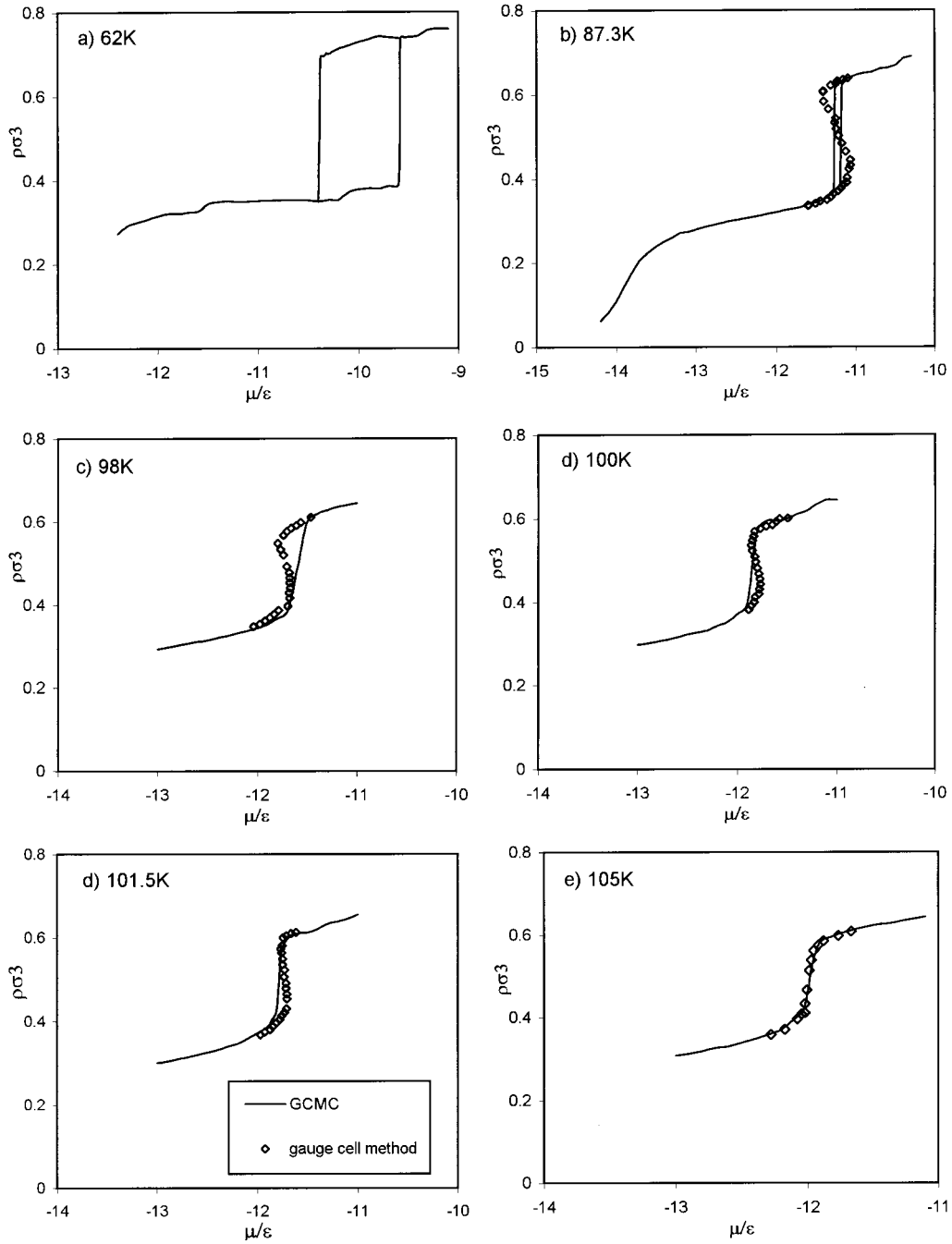

Figure 3. Argon adsorption isotherms in a 2.2 nm cylindrical pore obtained by the gauge cell and GCMC methods at different temperatures: (a) 62, (b) 87.3, (c) 98, (d) 100, (e) 101.5, and (f) 105 K.

trajectory (Figure 4). As expected, in the presence of fluctuations the phase transition step is rounded.

The sigmoid shape of the full adsorption isotherm flattens as the temperature increases further. At 101.5 K the isotherm obtained by the gauge cell method is almost vertical, indicating that the fluid is very close to the critical point (Figure 3e). At 105 K the full adsorption isotherm is monotonic and coincides with the GCMC isotherm, thus showing that this temperature is supercritical. From these data, we estimated the critical temperature for argon in this pore as 101.5 ± 2 K, which is close to experimentally obtained 98 K.[38] Taking into account all simplifying assumptions of the ideal pore model employed, possible pore size heterogeneity in the sample, inherent experimental errors, and the empirical method of the critical temperature determination used in ref 38, we conclude that the gauge cell method provides a quantitative estimate of the pore critical temperature.

3.2. Pore Size Dependence of Capillary Condensation. Determination of the Critical Conditions. The gauge cell method was employed to study sorption equilibria of Ar at its normal boiling temperature, 87.3 K, in a series of cylindrical pores of 5, 6, 7.265, 10.382, 11, 13, and 15.885 argon molecular diameters ($\sigma_{ff} = 0.34$ nm) in width, as measured between the centers of the outer oxygen atom layers at the opposite pore walls. The internal pore diameters, reduced by the oxygen diameter $\sigma_s = 0.27$ nm, are 1.43, 1.77, 2.20, 3.13, 3.60, 4.15, 5.12, and 5.54 nm, respectively. The last five pores represent typical channels in the MCM-41 type samples studied experimentally.[40−43] The mean pore diameters of these samples

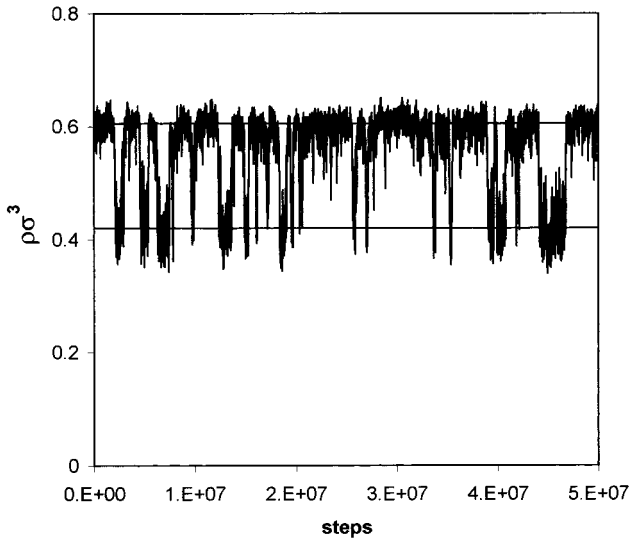

Figure 4. Dependence of the density throughout a 5×10^7 step GCMC simulation run in a 2.2 nm cylindrical pore at 98 K in the vicinity of the vapor−liquid equilibrium in a pore ($P/P_0 = 0.045$). The horizontal solid lines show the densities of equilibrium vaporlike and liquidlike phases, estimated using the gauge cell method.

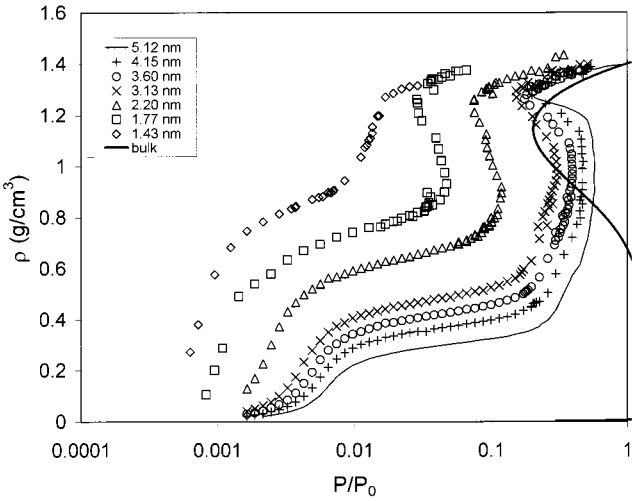

Figure 5. Calculated argon adsorption isotherms in a series of cylindrical pores of different widths at 87.3 K. The results of the gauge cell and GCMC methods are merged together into the full adsorption isotherms, which include stable, metastable, and unstable states. The thick solid line represents the bulk isotherm calculated by the equation of Johnson et al.[28]

were determined from N_2 and Ar adsorption isotherms using the NLDFT method.[40]

Figure 5 shows the full adsorption isotherms in the pores of diameters 1.43, 1.77, 2.20, 3.26, 3.47, 4.15, and 5.12 nm. The isotherm of bulk LJ argon calculated using the equation of Johnson et al.[28] is presented for comparison. The isotherms (with the exception of the narrowest pore of 1.43 nm) have a sigmoid shape characteristic of the first-order phase transition. The backward region of the isotherm corresponds to unstable states with negative compressibility. In the 1.43 nm wide pore, which can accommodate only two concentric adsorbed layers, the adsorption isotherm is monotonic, indicating that the fluid in this pore is supercritical: No phase separation and, consequently, no first-order transition occur in the process of condensation. This regime of supercritical sorption is known in adsorption literature as volume filling.[44] Thus, the critical width of cylindrical siliceous pores with respect to argon at 87.3 K lies between 1.43 and 1.77 nm.

It is instructive to compare the results obtained by the gauge cell and GCMC methods (Figure 6). In the supercritical pore of 1.43 nm, the GCMC data coincide with the monotonic isotherm, obtained by the gauge cell method. However, in the 1.77 nm pore the GCMC isotherm is continuous and monotonic while the isotherm obtained by the gauge cell method is sigmoid, which indicates the first-order condensation transition in this pore. On the basis of the gauge cell calculations, we conclude that the fluid in this pore is subcritical at 87.3 K. The GCMC isotherm represents a rounded step due to prominent density fluctuations in the vicinity of the critical pore point. The fluid densities obtained by averaging the GCMC configurations in the vicinity of the equilibrium transition points resulted from frequent jumps from vaporlike states to liquidlike states and back, similar to those described in section 3.1. As the pore width increases, the potential barrier between the vaporlike and liquidlike states becomes higher, and the "jumps" disappear. The GCMC isotherms for the larger pores (2.20, 3.13, 3.60, 4.15, 5.12, 5.54 nm) exhibit discontinuities associated with spontaneous capillary condensation and desorption and form prominent hysteresis loops. The spontaneous transitions during the GCMC simulations occur prior to the achievement of the spinodal. The pressures corresponding to spontaneous irreversible condensation and desorption are notably different from the vaporlike and liquidlike spinodal pressures, obtained by the gauge cell method. As the pore size increases, the deviation between the point of spontaneous transition observed in the GCMC simulation and the spinodal achieved in the gauge cell method decreases.

3.3. Pore Size Dependence of the Equilibrium and Spinodal Transitions. From the sigmoid adsorption isotherms, the conditions of phase coexistence, the densities of the equilibrium vaporlike and liquidlike states, and the spinodal pressures were determined. The pressures of the equilibrium and spinodal transitions vs the pore width are given in Figure 7. One expects that these functions merge together at the critical pore size and then monotonically increase approaching different asymptotics: the equilibrium pressure has to approach the Kelvin equation for the spherical meniscus, $P/P_0 = \exp(-2\sigma v/RTr)$; the vaporlike spinodal pressure of spontaneous condensation has to approach the Kelvin equation for the cylindrical meniscus, $P/P_0 = \exp(-\sigma v/RTr)$; the liquidlike spinodal pressure has to come to a plateau approaching the bulk liquid spinodal pressure. The range of pore sizes considered is too narrow to trace the asymptotic behavior of the equilibrium and spinodal condensation transitions. Even for the widest pore considered (5.54 nm), the equilibrium was observed at $P/P_0 = 0.54$, far away from bulk saturation. At the same time, the trend for the liquidlike spinodal is quite pronounced and for the widest pore of 5.54 nm the pressure of the liquidlike spinodal is close to that of the bulk liquid spinodal.

In Figure 8, we present the pore size dependence of the densities of liquidlike states in the subcritical pores (1.77 nm and wider) corresponding to the spinodal, equilibrium, and saturation conditions. The densities in the pores slightly fluctuate due to the ability to accommodate a certain number of adsorbed layers in a given pore. The packing effect is expected to be more prominent in smaller pores. It is noteworthy that the spinodal density does not vary appreciably and constitutes ca. 92% of the bulk saturated liquid density; that exceeds significantly the bulk spinodal density. The latter constitutes 82% of the bulk saturated liquid density. The pore equilibrium density increases with the pore size and is close to the saturated liquid density in pores wider than 4 mn. For comparison, we present

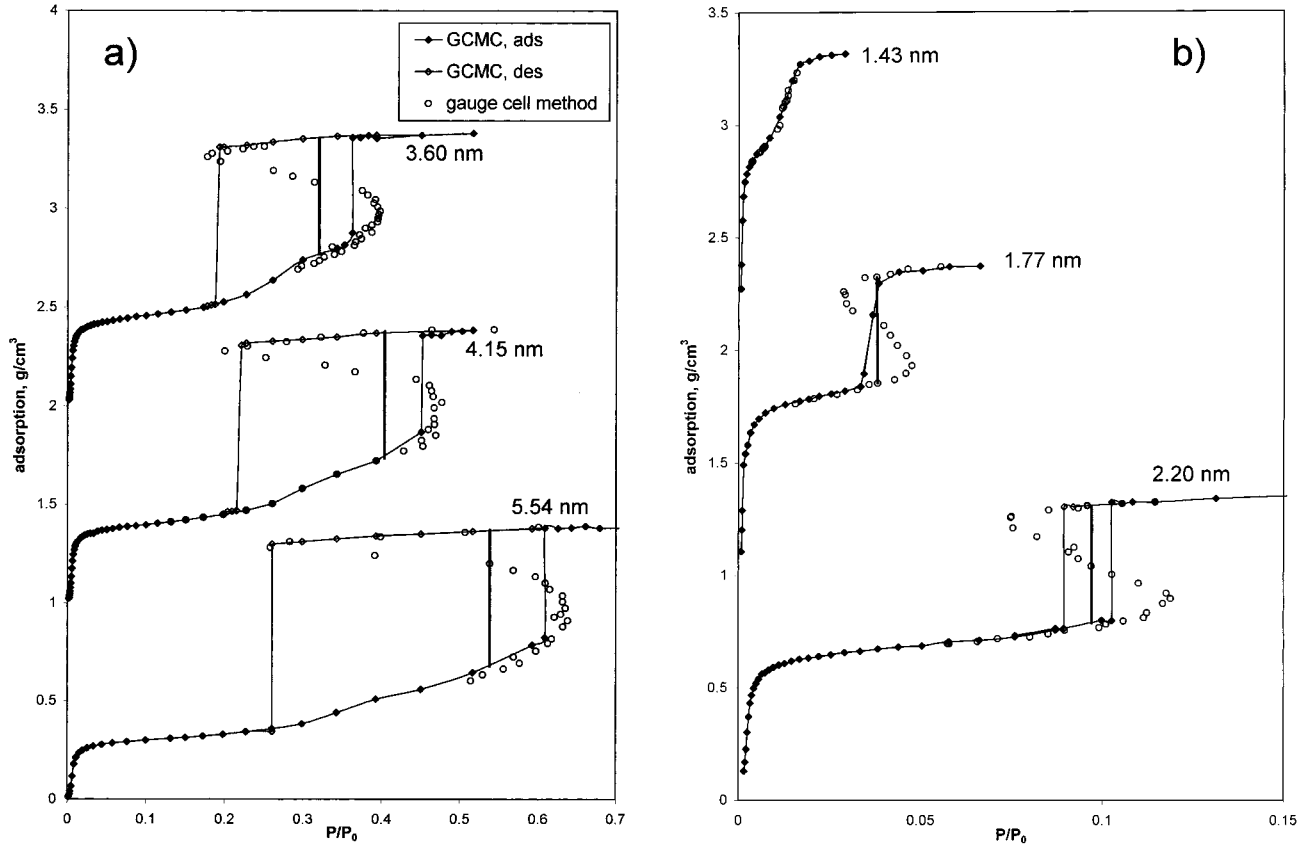

Figure 6. Calculated argon adsorption isotherms in cylindrical pores of different sizes at 87.3 K, obtained by gauge cell and GCMC methods. Thin vertical steps in the pores of 2.2 nm and wider indicate spontaneous condensation and desorption transitions observed in the GCMC simulations. Thick solid vertical lines indicate the vapor−liquid equilibrium in pores established by the gauge cell method.

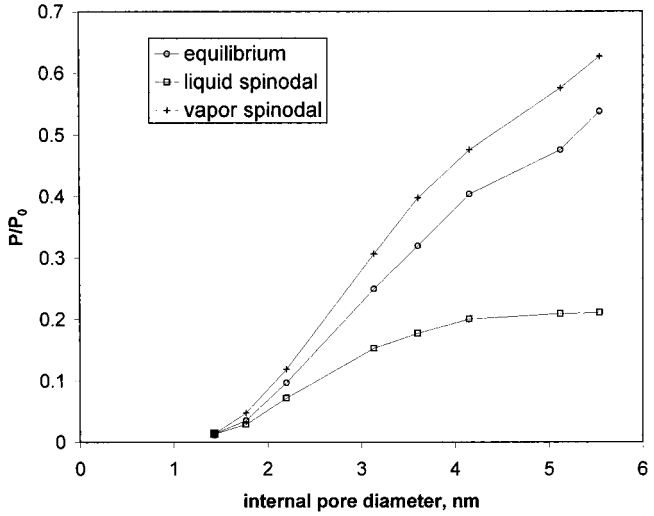

Figure 7. Pore size dependence of the pressures of liquidlike spinodal, vaporlike spinodal, and vapor−liquid equilibrium for argon sorption in cylindrical pores at 87.3 K.

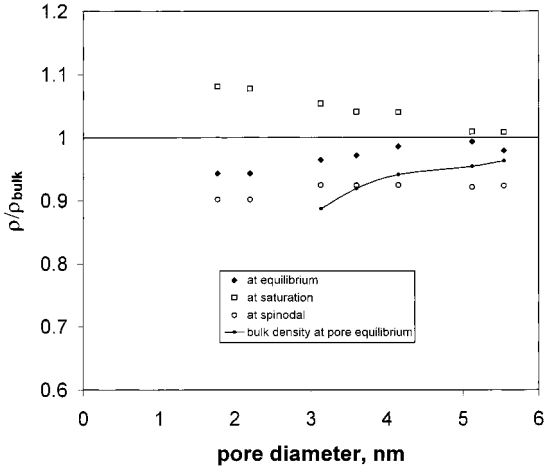

Figure 8. Densities of the confined liquid argon at 87.3 K in cylindrical pores at different conditions: pore vapor−liquid equilibrium (closed diamonds), bulk saturation pressure (open squares), and liquidlike spinodals (open circles). The solid line shows the densities of the bulk liquid at the conditions of vapor−liquid equilibrium in the pores. All densities are reduced by the bulk liquid density at saturation.

the bulk liquid density at the pressures corresponding to the pore equilibrium. The compressibility of the condensed fluid in all pores is substantial yet lower than that of the bulk liquid. The pore liquid densities at saturation are larger than the bulk density. For pores wider than 5 nm this deviation is practically negligible. However, for pores of 2−4 nm the deviations of the condensed fluid density from the bulk density exceed 5% and are to be taken into account while determining the pore volume from the adsorption data.

3.4. Pore Size Dependence of the Adsorption Film Formation prior to Condensation. Figure 9 shows the adsorption branches of argon adsorption isotherms. The relative pressures were determined from the chemical potentials (GCMC method) and the densities of the equilibrium bulk phase (GCGEMC method) via the equation of state for bulk LJ fluid by Johnson et al.[28] The isotherms show the formation of an adsorbed monolayer on the pore wall. The narrower the pore, the stronger the adsorption potential. Thus monolayer formation starts at a lower pressure in a narrower pore. However, the density of the adsorbed monolayer is essentially similar in all the pores considered, so that the isotherms in different pores almost

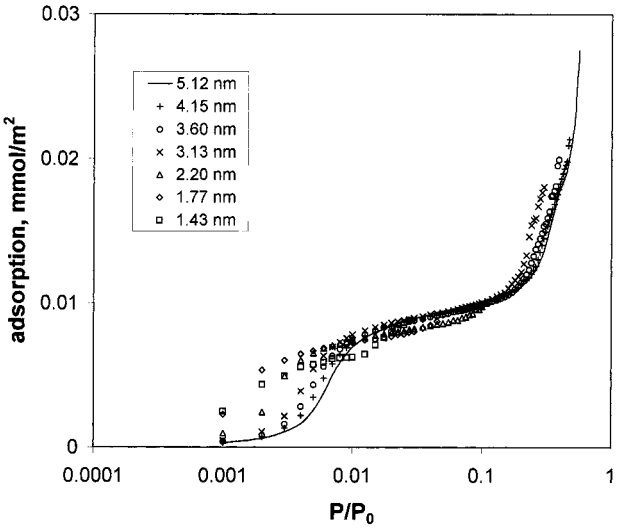

Figure 9. Adsorption branches of the GCMC argon adsorption isotherms in cylindrical pores of different sizes at 87.3 K.

coincide in the 0.01−0.1 relative pressure range. In the 2.20, 1.77, and 1.43 nm pores, the entire pore space is filled by the condensed fluid before the second monolayer forms. In the wider pores of 5.54, 5.12, 4.15, 3.60, and 3.13 nm width, the formation of second and even third adsorbed layers is observed prior to the capillary condensation. Similar to the first layer, the second one is formed at a lower pressure in a narrower pore. There are notable deviations between the isotherms in different pores at the stage of the second and third monolayer formation ($0.2 < P/P_0 < 0.5$) (Figure 9).

4. Comparison with Experiment

While comparing the simulation and experimental data, one has to recognize that the theoretical isotherms were constructed at special conditions where possible density fluctuations in the confined fluid were minimized. The severe suppression of density fluctuations allowed us to visualize the metastable and even unstable states, which would not be observed without special precautions. This means that, under real conditions, one may expect to observe the stable states and only those metastable states which are separated from the stable states by energy barriers that are too high to be overcome within the period of observation. The theoretical spinodals determine the true limits of stability of the metastable phases and, consequently, the upper and lower limits of experimentally observable phase transitions. As related to the capillary condensation/evaporation in open-ended cylindrical pores, it is well documented that metastable liquidlike states are not observed since, as the vapor pressure decreases, evaporation occurs at the equilibrium via formation of the meniscus at the pore edge.[45,46] At the same time, depending on the pore size, metastable vaporlike states can be monitored experimentally and therefore condensation may occur irreversibly as the spontaneous transition from a metastable state to a stable state, giving rise to the hysteresis. In the adsorption literature this effect is referred to as "delayed condensation".[47] When the delayed condensation occurs close to the vaporlike spinodal, it is said that the condensation proceeds in the *regime of developed hysteresis*.[47] The transient *regime of developing hysteresis*[15] takes place when spontaneous condensation occurs within an appreciable distance from the spinodal, so that the experimental hysteresis loop is narrower than the theoretical one limited by the spinodal. According to this classification, four regimes of sorption in cylindrical nanopores are distinguished depending on the pore size and[15] (1) supercritical sorption without phase separation (regime of pore volume filling), (2) reversible condensation with phase separation (first-order phase transition without hysteresis), (3) irreversible condensation with developing hysteresis, and (4) irreversible condensation with developed hysteresis.

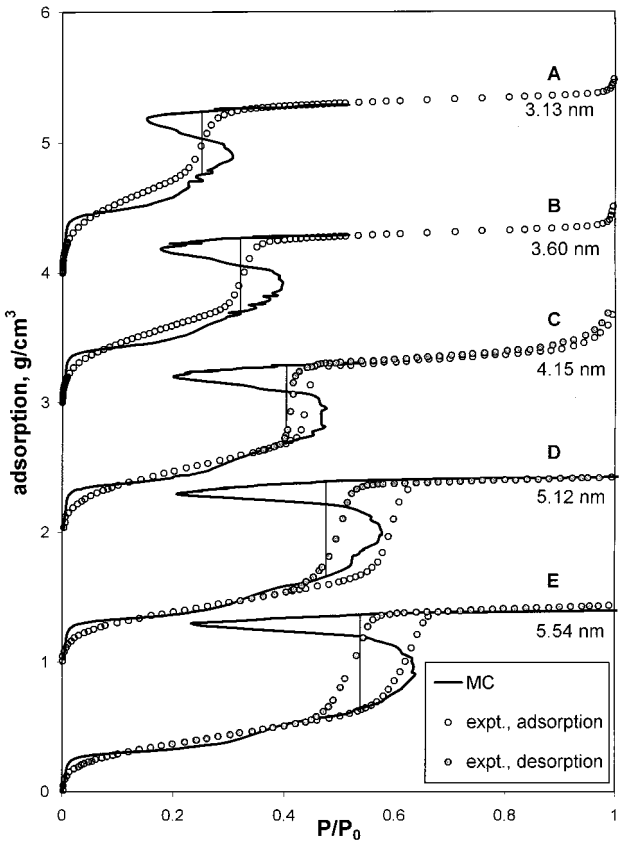

Figure 10. Monte Carlo argon adsorption adsorption isotherms in cylindrical pores (pore width shown on the plot) and experimental argon adsorption isotherms in the corresponding MCM-41 samples at 87.3 K (denoted as A−E; experimental data from refs 37, 41, and 42—see section 4 for description). The results of the gauge cell and GCMC methods are blended together into the full MC adsorption isotherms, which include stable, metastable, and unstable states. Thin solid vertical lines show the location of vapor−liquid equilibrium established by the gauge cell method.

Figure 10 shows the comparison of the full adsorption isotherms calculated by the gauge cell method and the experimental adsorption and desorption isotherms of argon at 87.7 K on the samples of MCM-41 type materials. For convenience of presentation, the adsorbed amount is reduced per unit pore volume. The typical pore size in these materials, as determined by the NLDFT method,[34,40,41] corresponds to the width of the model pore in which the simulation was performed. The pore volume of the samples was also determined by the NLDFT method from the experimental isotherms. The samples are designated as A (h = 3.13 nm [41]), B (h = 3.6 nm [41]), C (h = 4.15 nm[37]), D (h = 5.12 nm[42]), and E (h = 5.54 nm [42]).

Since the pore model with an energetically uniform, structureless wall cannot capture the intrinsic molecular heterogeneity of silica surface, the calculated isotherms deviate from the experimental ones in the region of adsorption film formation prior to the region of capillary condensation. This deviation is more pronounced in the narrower pores. However, the adsorbed film smooths the surface heterogeneity and in the region of condensation the correlation between the calculations and experimental data becomes apparent. Indeed, for sample E with

the widest pores, the calculated adsorption branch of the isotherm is in good agreement with the experimental isotherm up to the theoretical vaporlike spinodal point.

The data presented in Figure 10 demonstrate three regimes of capillary condensation. The *regime of reversible capillary condensation* is observed for samples A and B, the experimental isotherms of which do not show hysteresis. Instead of vertical steps characteristic to condensation/evaporations in a single pore, the experimental isotherms are rounded due to the narrow yet appreciable pore size distribution in the samples. The characteristic positions of the condensation transition can be estimated from the inflection points of the experimental isotherms. It is seen that experimental and calculated pressures of equilibrium capillary condensation, as well as the condensed liquid density, agree very well for both samples.

From the absence of hysteresis, it does not follow by any means that the sorption is supercritical as was assumed in earlier interpretations of the capillary condensation data.[48] This conclusion has been for the first time formulated by Ravikovitch et al.[35] based on the comparison of density functional theory predictions with experiments on nitrogen sorption on reference mesoporous molecular sieves. For the range of pores existing in these samples, the critical temperature is substantially higher than 87.3 K. Indeed, Morishige and Shukimi[38] estimated the capillary critical temperature in a sample with the typical pore size of 2.2 nm as 98 K, while the capillary condensation hysteresis in this sample was not observed above 62 K; see section 3.1. Since the critical temperature is known to rise as the pore width increases, we must expect that in the pore wider than at least 2.2 nm the condensation is subcritical.

The regime of developed hysteresis is characteristic of capillary condensation in samples D and E. Capillary condensation occurs spontaneously very close to the vaporlike spinodal. "Very close" means "within a reasonable error bar" due to inherent experimental and computational errors. The regime of developing hysteresis ($r = 4-5$ nm) is observed for sample C. The vaporlike spinodal is not achieved experimentally, and spontaneous condensation occurs between the equilibrium and the spinodal. The experimental hysteresis loop is narrower than the maximum possible one bounded by the spinodal. For all hysteresis isotherms, evaporation/desorption occurs at the equilibrium similar to the reversible isotherms in the smaller pore size samples A and B. This confirms the general statement that in the open-ended cylindrical pores desorption occurs at the equilibrium conditions.

The results presented in Figure 10 confirm the estimate of the upper and lower limits of different regimes of condensation made in our previous work based on nitrogen sorption experiments. The regime of developed hysteresis is expected in pores greater than ca. 5 nm; the regime of reversible condensation is limited to pores less than ca. 4 nm; the regime of developing hysteresis takes place in the pores of intermediate size, ca. 4−5 nm. Although we are not aware of corresponding experimental data, the upper limit of supercritical sorption, ca. 1.8 nm, found by the gauge cell method, seems to be realistic. It also agrees with the estimate of the critical pore size obtained for nitrogen sorption earlier by the density functional theory method.[35]

5. Potential Barriers between the Metastable and Stable Equilibrium States

In the hysteresis region, the transition from a metastable state to a stable state is associated with the overcoming of an energy barrier. When the energy barrier can be overcome due to allowed density fluctuations in the pore, this transition occurs spontaneously. In the gauge cell simulations, the density fluctuations are suppressed and the spontaneous transitions are not observed. In the GCMC simulations, the probability of a spontaneous transition depends on the height of the energy barrier. We hypothesize that the height of the energy barrier can be estimated by the grand potential at the saddle points, which correspond to the backward trajectory of the phase diagram. This hypothesis implies that at a given chemical potential μ the energy barrier is proportional to the difference of the grand potentials in the unstable state on the backward trajectory and in the metastable state:

$$\Delta\Omega^*(\mu) = \Omega_u(\mu) - \Omega_a(\mu), \mu > \mu_e(\text{condensation}) \quad (11a)$$

$$\Delta\Omega^*(\mu) = \Omega_u(\mu) - \Omega_d(\mu), \mu < \mu_e(\text{evaporation/desorption}) \quad (11b)$$

The grand potentials along the adsorption, $\Omega_a(\mu)$, desorption, $\Omega_d(\mu)$, and unstable, $\Omega_u(\mu)$, branches are calculated by thermodynamic integration (eq 8).

The potential barrier vanishes at the spinodals and achieves a maximum at the point of phase coexistence. For the case of the cylindrical pores considered in our simulations, it is convenient to operate with a potential barrier reduced per unit pore length. In so doing, the probability of the spontaneous transition is proportional to the Arrhenius factor given by

$$P^*(\mu) = \exp(-l\Delta\Omega(\mu)/kT) \quad (12)$$

Here, l is a characteristic length, which depends on the longitudinal scale of the developing fluctuation. Physically, this fluctuation in the process of condensation can be imagined as a film undulation transforming into a liquid bridge, which spans the pore. The process of spontaneous evaporation/desorption starts from the coalescence of intermolecular cavities into a "bubble". The longitudinal scale of such density fluctuations is likely to be of the order of the pore width. Correspondingly, in the estimates presented below, the characteristic scale in the Arrhenius factor (eq 12) is assumed to be equal to the pore width.

The possibility of analyzing the potential barriers and the probability of spontaneous transitions is an additional advantage of the proposed gauge cell method. This constitutes a basis for formulations of the conditions of the reversibility of simulated and experimental adsorption isotherms. We calculated the Arrhenius factors (eq 12) for all pores where the capillary condensation is subcritical. They are presented in Figure 11. At the vaporlike spinodal point, the Arrhenius factor (and, therefore, the probability of spontaneous condensation) is equal to 1. The lowest value of the Arrhenius factor corresponds to the point of the vapor−liquid equilibrium in the pores. The minimum of the Arrhenius factor drops drastically as the pore width increases, and can be as small as 10^{-47}. The large potential barrier makes reversible transitions between the liquidlike and vaporlike states in the GCMC simulations impossible in pores wider than 1.77 nm. Figure 11 shows the locations of irreversible vapor-to-liquid and liquid-to-vapor transitions in GCMC simulations. It is seen that the transitions correspond to the points were the Arrhenius factor P^* exceeds $10^{-3}-10^{-1}$ in all pores. This outlines an approximate potential barrier that may be overcome due to fluctuations inherent to the GCMC simulations. The adsorption hysteresis in the GCMC simulations widens as the potential barrier gets larger with the increase of the pore size.

It is worth noting that in the GCMC simulations reported the density fluctuations, though allowed, are still essentially

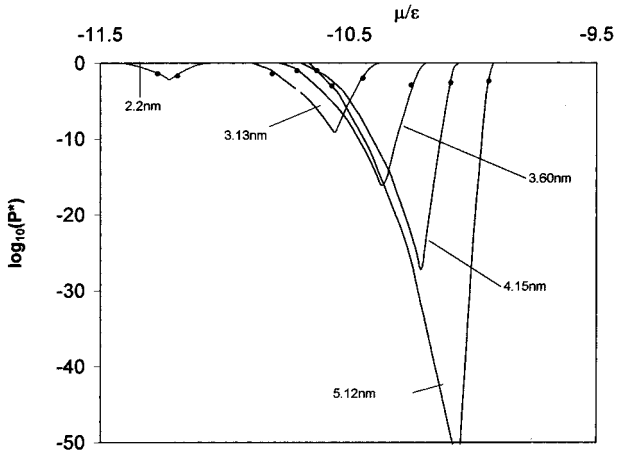

Figure 11. Arrhenius factors for the spontaneous capillary condensation/desorption of argon in cylindrical pores of different sizes at 87.3 K. Points on the lines show the locations of spontaneous condensation and desorption transitions in GCMC simulations.

suppressed. A limited size of the simulation cell dictates the fluid homogeneity in the direction parallel to the walls. At experimental conditions, the level of density fluctuations is expected to be much higher than in simulations, primarily due to inevitable temperature fluctuations and a structural inhomogeneity of samples. This explains the apparent absence of hysteresis for samples A−C with the characteristic pore width 2.2−3.47 nm, for which hysteresis would be expected based on the GCMC simulations showing visible irreversibility (Figure 10). Since the potential barrier increases sharply with the pore size, the level of allowed fluctuation has a lower impact in wider pores. As a result, in the pores exhibiting the developed hysteresis (samples D and E), the experimental and the GCMC capillary condensation isotherms are in good agreement.

6. Conclusions

The gauge cell method is proved to be efficient for MC simulation of adsorption isotherms, determination of the conditions of vapor−liquid equilibrium and criticality in pores, estimation of the true limits of stability of liquidlike and vaporlike states, and evaluation of potential barriers associated with capillary condensation and desorption in pores. The method allows one to calculate the full sorption isotherm, which at subcritical conditions has a sigmoid shape similar to the van der Waals isotherms. The capabilities of the gauge cell method were demonstrated on argon adsorption in a series of cylindrical pores, which represent typical pore channels of MCM-41 molecular sieves. The temperature dependence of capillary condensation in the 2.2 nm pore and the pore size dependence of capillary condensation at argon normal boiling temperature, 87.3 K, were explored.

The results of the gauge cell method were compared with those obtained by the conventional GCMC method. At supercritical and subcritical conditions the GCMC data agree well with the gauge cell method data. However, in the vicinity of the critical point and at subcritical conditions close to the spinodals, the gauge cell method reveals states which are not achieved in the GCMC simulation. In particular, the limits of stability of vaporlike and liquidlike states in GCMC simulations are shown to differ from the true limits of the metastable state stability, the vaporlike and liquidlike spinodals. In the vicinity of the pore critical temperature, the GCMC method produces a monotonic reversible isotherm, resulting from relatively frequent jumps between vaporlike and liquidlike states, while the vapor−liquid equilibrium can still be determined by the gauge cell method. It is shown that the condensed liquid densities in pores differ from the bulk liquid density for pores narrower than 5 nm. However, for pores of 2−4 nm the deviations of the condensed fluid density from the bulk density exceed 5% and are to be taken into account while determining the pore volume from the adsorption data.

The probability of spontaneous transitions between metastable and stable states was analyzed based on the energy barriers. The Arrhenius factor for such a transition was estimated. For the spontaneous transitions observed in the GCMC simulations the Arrhenius factors were found to be as large as $10^{-3}-10^{-1}$. In the regime of developed hysteresis, the Arrhenius factors can be as small as 10^{-47}. A further analysis of the energy barriers between metastable and stable states can shed light on the quantification of the hysteresis regimes observed experimentally. This implies a study of nucleation phenomena associated with symmetry breaking of the translation invariant solutions.

We compared the calculated MC adsorption isotherms with experimental data on argon sorption for a series of samples of mesoporous molecular sieves of MCM-41 type and found consistent agreement between the experimental desorption pressures and the calculated pressures of vapor−liquid equilibrium in pores. In pores wider than 5 nm, which exhibit adsorption−desorption isotherms with developed hysteresis, we observed good agreement between the experimental pressure of capillary condensation and the calculated spinodal condensation pressure.

Although a strict statistical mechanical analysis of the gauge cell method and its limitations is still in the works, agreement with the proven techniques of GCMC and GEMC simulations and also with reference experiments is quite convincing. The gauge cell method is recommended for studies of other equilibrium processes and phase transitions in confined systems such as multicomponent sorption, phase separation, dewetting of thin films, nucleation, and the like.

References and Notes

(1) Neimark, A. V.; Vishnyakov, A. *Phys. Rev. E* **2000**, *62*, 4611.
(2) Vishnyakov, A.; Piotrovskaya, E. M.; Brodskaya, E. N. *Adsorpt.-J. Int. Adsorpt. Soc.* **1998**, *4*, 207.
(3) Segarra, E. I.; Glandt, E. D. *Chem. Eng. Sci.* **1994**, *49*, 2953.
(4) Peterson, B. K.; Gubbins, K. E. *Mol. Phys.* **1987**, *62*, 215.
(5) Wilding, N. B.; Schoen, M. *Phys. Rev. E* **1999**, *60*, 1081.
(6) Panagiotopoulos, A. Z. *Mol. Phys.* **1987**, *62*, 701.
(7) Bojan, M. J.; Steele, W. A. *Carbon* **1998**, *36*, 1417.
(8) Samios, S.; Stubos, A. K.; Kanellopoulos, N. K.; Cracknell, R. F.; Papadopoulos, G. K.; Nicholson, D. *Langmuir* **1997**, *13*, 2795.
(9) Gac, W.; Patrykiejew, A.; Sokolowski, S. *Surf. Sci.* **1994**, *306*, 434.
(10) Gozdz, W. T.; Gubbins, K. E.; Panagiotopoulos, A. Z. *Mol. Phys.* **1995**, *84*, 825.
(11) Kierlik, E.; Rosinberg, M.; Finn, J. E.; Monson, P. A. *Mol. Phys.* **1992**, *75*, 1435.
(12) Radhakrishnan, R.; Gubbins, K. E.; Sliwinska-Bartkowiak, M. *J. Chem. Phys.* **2000**, *112*, 11048.
(13) Miyahara, M.; Gubbins, K. E. *J. Chem. Phys.* **1997**, *106*, 2865.
(14) Gelb, L. D.; Gubbins, K. E.; Radhakrishnan, R.; Sliwinska-Bartkowiak, M. *Rep. Prog. Phys.* **1999**, *62*, 1573.
(15) Neimark, A. V.; Ravikovitch, P. I.; Vishnyakov, A. *Phys. Rev. E* **2000**, *62*, R1493.
(16) Penrose, O.; Lebowitz, J. L. *J. Stat. Phys.* **1971**, *3*, 211.
(17) Reiss, H. *Ber. Bunsen-Ges. Phys. Chem. Chem. Phys.* **1975**, *79*, 943.
(18) Penrose, O.; Lebowitz, J. L. Towards a rigorous molecular theory of metastability. In *Fluctuation Phenomena*; Lebowitz, J. L., Montroll, E., Eds.; North Holland: Amsterdam, 1987.
(19) Corti, D. S.; Debenedetti, P. G. *Chem. Eng. Sci.* **1994**, *49*, 2717.
(20) Hill, T. L. *Thermodynamics of Small Systems*; W. A. Benjamin, Inc.: New York, 1963.
(21) Dekeizer, A.; Michalski, T.; Findenegg, G. H. *Pure Appl. Chem.* **1991**, *63*, 1495.

(22) Gusev, V. Y. Monte Carlo Simulations of Fluid Phase Transitions in Micropores: Hysteresis and van der Waals-type Loops. In *Microscopic Simulation of Interfacial Phenomena in Solids and Liquids*; Phillpot, S. R., Bristowe, P. D., Stroud, D. G., Smith, J. R., Eds.; Materials Research Society: Warrendale, PA, 1998; Vol. 492; p 35.
(23) Binder, K. J. *Non-Equilib. Thermodyn.* **1998**, *23*, 1.
(24) Landau, L. D.; Lifshitz, E. M. *Statistical Physics*; Pergamon: Oxford, 1959; Vol. 1.
(25) Privman, V.; Fisher, M. E. *J. Stat. Phys*. **1983**, *33*, 385.
(26) Fisher, M. E. *J. Phys. Soc. Jpn.* **1969**, *S26*, 87.
(27) Binder, K. *Annu. Rev. Phys. Chem*. **1992**, *43*, 33.
(28) Johnson, J. K.; Zollweg, J. A.; Gubbins, K. E. *Mol. Phys.* **1993**, *78*, 591.
(29) Vishnyakov, A.; Debenedetti, P. G.; Neimark, A. V. *Phys. Rev. E* **2000**, *62*, 538.
(30) Panagiotopoulos, A. Z.; Quirke, N.; Stapleton, M.; Tildesley, D. J. *Mol. Phys.* **1988**, *63*, 527.
(31) Gonzalez, A.; White, J. A.; Roman, F. L.; Velasco, S.; Evans, R. *Phys. Rev. Lett.* **1997**, *79*, 2466.
(32) Gonzalez, A.; White, J. A.; Roman, F. L.; Evans, R. *J. Chem. Phys.* **1998**, *109*, 3637.
(33) White, J. A.; Gonzalez, A.; Roman, F. L.; Velasco, S. *Phys. Rev. Lett.* **2000**, *84*, 1220.
(34) Ravikovitch, P. I., unpublished.
(35) Ravikovitch, P. I.; O'Domhnaill, S. C.; Neimark, A. V.; Schuth, F.; Unger, K. K. *Langmuir* **1995**, *11*, 4765.
(36) Tjatjopoulos, G. J.; Feke, D. L.; Mann, J. A. *J. Phys. Chem.* **1988**, *92*, 4006.
(37) Ravikovitch, P. I.; Wei, D.; Chueh, W. T.; Haller, G. L.; Neimark, A. V. *J. Phys. Chem. B* **1997**, *101*, 3671.
(38) Morishige, K.; Shikimi, M. *J. Chem. Phys.* **1998**, *108*, 7821.
(39) Forsman, J.; Woodward, C. E. *Mol. Phys.* **1997**, *90*, 637.
(40) Neimark, A. V.; Ravikovitch, P. I. *Micropor. Mesopor. Mater.* **2001**, *44*, 697.
(41) Neimark, A. V.; Ravikovitch, P. I.; Grun, M.; Schuth, F.; Unger, K. K. *J. Colloid Interface Sci.* **1998**, *207*, 159.
(42) Kruk, M.; Jaroniec, M. *Chem. Mater*. **2000**, *12*, 222.
(43) Ravikovitch, P. I.; Haller, G. L.; Neimark, A. V. *Adv. Colloid Interface Sci.* **1998**, *77*, 203.
(44) Dubinin, M. M. *Chem. Rev.* **1960**, *60*, 235.
(45) Everett, D. H. In *The Solid−Gas Interface*; Flood, E. A., Ed.; Marcel Dekker: New York, 1967; Vol. 2, Chapter 36.
(46) Evans, R. *J. Phys.: Condes. Matter* **1990**, *2*, 8989.
(47) Sing, K. S. W.; Everett, D. H.; Haul, R. A. W.; Moscou, L.; Pierotti, R. A.; Rouquerol, J.; Siemieniewska, T. *Pure Appl. Chem.* **1985**, *57*, 603.
(48) Ball, P. C.; Evans, R. *Langmuir* **1989**, *5*, 714.